Nuclear Instruments and Methods in Physics Research A 338 (1994) 166–184
North-Holland

NUCLEAR INSTRUMENTS & METHODS IN PHYSICS RESEARCH
Section A

High spin polarization at the HERA electron storage ring

D.P. Barber [a], M. Böge [a], H. Böttcher [b], H.-D. Bremer [a], R. Brinkmann [a], W. Brückner [c], M. Düren [c], E. Gianfelice-Wendt [a], R. Kaiser [a], R. Klanner [a], H.-Ch. Lewin [a], M. Lomperski [d], N. Meyners [a], W.-D. Nowak [b], P.M. Patel [e], G. Ripken [a], K. Rith [f], H.O. Roloff [b], E. Steffens [c], D. Westphal [g], K. Zapfe [a], F. Zetsche [g]

[a] *Deutsches Elektronen-Synchrotron DESY, Hamburg, Germany*
[b] *DESY – Institut für Hochenergiephysik, Zeuthen, Germany*
[c] *Max Planck Institut für Kernphysik, Heidelberg, Germany*
[d] *University of Wisconsin, Madison, Wisconsin, USA*
[e] *McGill University, Montreal, Canada*
[f] *University of Erlangen – Nürnberg, Erlangen, Germany*
[g] *University of Hamburg, Hamburg, Germany*

(Received 8 June 1993)

This paper describes the progress made in 1992 towards increasing the vertical electron beam polarization at HERA. Utilizing harmonic spin-orbit corrections and beam tuning, the vertical polarization has been increased from 15% to nearly 60% at a beam energy of 26.7 GeV. The long-term reproducibility of the polarization is excellent. Measurements of the build-up time and the energy dependence of the polarization are also described.

1. Introduction

The HERA electron–proton colliding beam facility was designed with the aim of storing polarized electrons. The stored beam can become vertically polarized through the emission of synchrotron radiation in the arcs. Spin rotators in the straight sections can be utilized to provide longitudinal spin polarization at the interaction points. The first pair of spin rotators [1] will be installed in early 1994.

Vertical polarization of the electron beam at the 8% level was observed in November 1991 at the current operating energy of 26.7 GeV. The HERA polarimeter and these first measurements are described in detail in ref. [2]. The following steps were taken to increase the polarization:

- the alignment of the quadrupole magnets was checked and selected magnets were realigned,
- the tilt of the electron beam ellipse was corrected with an orbit bump distributed around the ring,
- the orbital tunes were changed to increase the energy separation of the first order betatron resonances,
- the harmonic spin–orbit correction scheme was prepared and tested with simulations.

Parasitic measurements in April and June 1992 showed that owing to the first two steps the maximum polarization had increased to about 18%. After optimization of the orbit corrections nearly 60% vertical polarization was obtained. Preliminary results can be found in ref. [3]. This paper details the preparations made to increase the expected polarization, in particular the harmonic spin–orbit correction scheme; the improvements made to the polarimeter since November 1991; and the results of the orbit correction studies and other measurements performed during August and September 1992.

2. The harmonic spin–orbit corrections

2.1. Polarization in storage rings

2.1.1. The Sokolov–Ternov process

A stored electron beam becomes spin polarized through the emission of synchrotron radiation. This effect was first predicted by Sokolov and Ternov [4], who considered the case of electrons moving in a plane, perpendicular to a uniform, constant magnetic

SSDI 0168-9002(93)E0521-S

field [#1]. The polarization P builds up in time according to ref. [5]

$$P(t) = P_{ST}(1 - e^{-t/\tau_{ST}}), \tag{1}$$

where τ_{ST} is the polarization build-up time and P_{ST} is the equilibrium polarization. The polarization direction is antiparallel to the guide field, and the asymptotic value, P_{ST}, is 92.4%. The build-up time is a strong function of the beam energy and the bending radius of the magnetic field ρ:

$$\tau_{ST} = \left(\frac{5\sqrt{3}}{8} \frac{c\lambda\!\!\!^{-}_c r_0 \gamma^5}{\rho^3} \right)^{-1}, \tag{2}$$

where $\lambda\!\!\!^{-}_c$ and r_0 are the reduced Compton wavelength and the classical radius of the electron.

In real electron storage rings the magnetic fields experienced by the beam are much more complicated than assumed in the Sokolov–Ternov case, being designed so as to confine the electron orbits and containing unavoidable misalignments and field errors. In addition to causing spin-flip with very low probability [5], the emission of synchrotron radiation produces stochastic kicks of the energy of the electrons owing to the discrete nature of the photon emission. These kicks can, in a real storage ring, lead to a diffusion of the spins and thus play an important role in determining the achievable polarization level in a real ring. A complete description of the polarization process in real machines, which includes these effects in a unified way, requires a quantum mechanical formulation which treats the orbital and spin motion in the semiclassical limit [6,7]. For our purposes here, it is sufficient and illuminating to divide the description into two separate processes, namely the build-up of polarization by the Sokolov–Ternov effect, described using quantum mechanics; and the depolarization due to spin diffusion, resulting from the classical stochastic motion of the stored electrons.

The discussion begins with the equation of motion of the spins in the magnetic confining field. The polarization vector $\boldsymbol{P}$, defined in the rest frame of a relativistic electron in a storage ring, precesses according to the Thomas–BMT equation [8]

$$\frac{d\boldsymbol{P}}{d\tau} = \frac{e\boldsymbol{P}}{m_e c\gamma} \times \left[(1 + a\gamma)\boldsymbol{B}_\perp + (1 + a)\boldsymbol{B}_\parallel \right],$$

$$a = \left(\frac{g - 2}{2} \right), \tag{3}$$

where $\boldsymbol{B}_\perp$, $\boldsymbol{B}_\parallel$ are the magnetic fields perpendicular and parallel to the trajectory, τ is the distance along the instantaneous particle direction, and g is the electron g-factor. The periodic solution of eq. (3) for a non-radiating electron on the periodic (closed) orbit is denoted by the unit vector $\hat{\boldsymbol{n}}_0(s)$. From turn to turn, the spins of particles on the closed orbit precess around $\hat{\boldsymbol{n}}_0(s)$ and the number of precessions per turn, the so-called spin tune, is denoted as ν. The $\hat{\boldsymbol{n}}_0$ axis is unique, provided that ν is not an integer.

The Sokolov–Ternov result has been generalized to the case of nonuniform fields, and can then be used to describe the build-up of the polarization of particles travelling on the closed orbit of a realistic storage ring [9,10]. The corresponding expression for the build-up time τ_{ST} is obtained from eq. (2) by replacing ρ with an effective bending radius ρ_{eff} [5]. In general, the periodic solution $\hat{\boldsymbol{n}}_0(s)$ is not everywhere vertical, as it is in the ideal Sokolov–Ternov case. It is also found that the equilibrium polarization direction is, in general, along $\hat{\boldsymbol{n}}_0$ and not along the local direction of the magnetic field.

In the case when there are no horizontal fields on the closed orbit ($B_x = B_\parallel = 0$) (and in addition when there are no reversed-field dipoles) the results are very similar to those in Sokolov–Ternov case: $\hat{\boldsymbol{n}}_0$ is vertical everywhere; the equilibrium polarization, P_{ST}, is equal to 92.4%; and the spin tune ν equals $a\gamma$, which at the HERA operating energy of 26.7 GeV is 60.5. The correction to the build-up time (2) is due to the drift spaces between bending magnets, and the effective bending radius ρ_{eff} is

$$\rho_{eff}^{-3} = \frac{1}{C} \oint \frac{ds}{|\rho(s)|^3}, \tag{4}$$

where C is the ring circumference and s is the distance along the design orbit. The corresponding build-up time τ_{ST} at HERA is 23 min at an energy of 30 GeV and 43 min at the current operating energy of 26.7 GeV.

In the case when horizontal fields are present on the closed orbit, the periodic solution $\hat{\boldsymbol{n}}_0$ is tilted away from the vertical and ν can deviate from $a\gamma$. If $\hat{\boldsymbol{n}}_0$ is not parallel to the vertical fields of the dipoles (where the Sokolov–Ternov effect occurs) then the build-up process is weakened, and the equilibrium polarization is less than the maximum value, P_{ST}. In most electron storage rings, including HERA, the design direction of $\hat{\boldsymbol{n}}_0$ is vertical in the dipoles, and the residual tilt due to field errors is small. The achievable asymptotic polarization of such a real ring can be significantly reduced as a result of the magnet misalignments, but this is not due to the weakening of the Sokolov–Ternov effect, but as will be explained, to the effects of the stochastic diffusion of the spins.

[#1] The reference frame we use has the dipole magnetic field along $\hat{y}$; in reality, due to the tilt of the HERA electron ring, this direction is 10 mrad from the vertical.

2.1.2. The spin diffusion process

The stochastic emission of synchrotron radiation excites oscillations of the stored particles about the closed orbit. When the fields on the closed orbit are not everywhere vertical, these oscillations can result in a diffusion of the spins. This process is most clearly described in an ideal example, in which the probability for spin-flip is neglected.

Consider a bunch of electrons initially on the closed orbit, with their spins aligned along the periodic axis $\hat{\boldsymbol{n}}_0$. If the electrons remain on this orbit, their spins remain aligned along $\hat{\boldsymbol{n}}_0$. The emission of synchrotron radiation excites energy oscillations, which, due to the vertical and horizontal dispersions, result in oscillations of the particles about the closed orbit. The magnetic fields (mainly in the quadrupoles) experienced by the particles off the closed orbit cause the spins to precess, according to eq. (3), away from their initial direction $\hat{\boldsymbol{n}}_0$. Because of the stochastic nature of the photon emission, the precession results in a diffusion of the spins, and hence, depolarization. The strength of this depolarizing process can be quantified with a time constant of the diffusion, τ_D. In this scheme, spin diffusion is considered to be working simultaneously with the Sokolov–Ternov build-up, and the value of the asymptotic polarization P_{max} is determined by the relative strengths of the two processes according to

$$P_{max} = P_{ST}\frac{\tau_D}{\tau_{ST}+\tau_D}. \tag{5}$$

Analogously, the equilibrium size of an electron bunch is determined by the relative strengths of the excitation and damping processes.

The effective build-up time τ is also reduced by spin diffusion, and τ_{ST} in eq. (1) must be replaced by

$$\tau = P_{max}\left(\frac{\tau_{ST}}{P_{ST}}\right). \tag{6}$$

For example at HERA at 26.7 GeV, with a τ_D of 10 min, the effective build-up time τ is 8 min and P_{max} is 0.18.

Spin diffusion is particularly strong (so that τ_D is small) when the precession of the spins is synchronous with the orbital and energy oscillations which drive the diffusion, i.e. when the spin resonance condition

$$\nu = m + m_x Q_x + m_y Q_y + m_s Q_s \tag{7}$$

is satisfied where Q_x, Q_y and Q_s are, respectively, the horizontal, vertical and synchrotron tunes of the machine and m and $m_{x,y,s}$ are integers. The strongest resonance systems for a typical ring are the first order resonances, with $|m_x|+|m_y|+|m_s|=1$. For a ring with high energy and large energy spread like HERA, the synchrotron sideband resonances are also strong, namely those with $|m_x|+|m_y|=1$ and m_s equal a small non-zero integer.

In this simplified picture the fraction of the total synchrotron radiation power which contributes to spin-flip is very small, but each synchrotron photon emitted can contribute to spin diffusion; thus, spin diffusion is a potentially strong effect, and the achievable polarization P_{max} may be much less than the maximum value, P_{ST}. It is important to calculate the resonance strengths and the polarization that one can expect in a real machine, and several computer codes are available. Linear approximations to the spin motion based on the program SLIM [5], which lead to the first order resonances, are often used as a guide, and analytic techniques [7,11] can be used to estimate higher order resonance effects. The spin diffusion process can also be simulated using Monte Carlo tracking programs, e.g. SITROS [12,13], allowing τ_D to be estimated under realistic conditions.

2.1.3. Controlling spin diffusion

Although spin diffusion effects are potentially strong, they can be minimized by paying proper attention to the design of the magnetic guide field and to the alignment of the magnets. In spite of these actions, spin diffusion in a real ring may still be strong, and the use of orbit correction schemes may be required. The discussion of methods of controlling spin diffusion can be clarified by defining the ring characteristics "flat" and "perfect".

– A ring is "flat" if, as in most electron storage rings, none of the main dipole magnets bends in the vertical plane (i.e. the dipole fields are vertical). Correction coils might be needed, though, to correct for vertical magnet misalignments. An important counter example will be the HERA ring after its spin rotators [1] are installed to achieve longitudinal polarization at the collision points.

– A ring is "perfect" if there are no magnetic field distortions due to magnet misalignments (tilts and displacements) or gradient errors. The dominant distortions in an "imperfect" ring are, in practice, the misalignments of quadrupoles.

An assumption we shall make, in order to simplify the discussion in this section, is that the ring contains no solenoids or skew quadrupoles.

If a ring is flat and perfect, then the $\hat{\boldsymbol{n}}_0$ axis is vertical, as in the ideal Sokolov–Ternov case. Furthermore the oscillations excited by the emission of synchrotron radiation are limited to the horizontal plane (i.e. there is no vertical dispersion). Thus the fields experienced by the electrons in the quadrupoles as they are stochastically excited off the closed orbit are vertical, N.B. parallel to the polarization direction $\hat{\boldsymbol{n}}_0$, so the oscillations produce no diffusion of the spins, i.e. $\tau_D = \infty$. Hence the asymptotic polarization P_{max} is equal to P_{ST}.

Horizontal magnetic fields are, by design, present on the closed orbit of a non-flat machine, thus the $\hat{n}_0$ axis is not vertical everywhere. An extreme case is that of a ring with spin rotators, which are used to rotate the polarization vector into the horizontal plane. In this case the tilt is 90°, but occurs only in a limited portion of the ring and is generated in a well defined manner. Two strong sources of spin diffusion are expected in a perfect, non-flat ring:

i) Because $\hat{n}_0$ is not vertical everywhere, the vertical fields of the quadrupoles experienced by electrons undergoing horizontal oscillations off the closed orbit are not everywhere parallel to $\hat{n}_0$. Thus, contrary to the case of a flat ring, the horizontal orbital oscillations can cause spin diffusion, and give rise to depolarizing resonances with $|m_x| = 1$ and m_s equal a small integer or zero, i.e. to (Q_x, Q_s) resonance systems.

ii) In addition, the horizontal fields on the closed orbit produce vertical dispersion, thus the energy oscillations excited by synchrotron radiation cause orbital oscillations in the vertical plane. The horizontal fields of the quadrupoles experienced by the electrons vertically off-set from the closed orbit are a source of spin diffusion even in positions where $\hat{n}_0$ is vertical. The vertical orbital motion gives rise to resonances with $|m_y| = 1$ and m_s equal a small integer or zero, i.e. to (Q_y, Q_s) resonance systems. Thus, the vertical bends in a non-flat ring can lead to strong spin diffusion due to the horizontal orbital motion combined with the tilt of $\hat{n}_0$, and due to the vertical orbital motion. These effects can be reduced by the special design of the optic, a technique called spin matching [1].

There is a limit to the precision to which the magnets can be positioned and oriented with respect to the design values and the deviations from the latter follow an approximately Gaussian distribution. For example, at HERA the rms transverse misalignments of the quadrupoles $\sigma_{x,y}$ are 0.3 mm, and the rms tilt errors $\sigma_{x',y'}$ are 0.35 mrad. The closed orbit of a nominally flat electron machine with misalignments does not lie in the horizontal plane. The rms distortion of the vertical closed orbit is reduced using vertical correction coils and orbit correction algorithms. The horizontal magnetic fields on the closed orbit, due to both the misalignments and the correction fields, tilt the periodic axis $\hat{n}_0$ from the design value and also cause vertical dispersion. Thus the two sources of spin diffusion discussed in the case of a perfect non-flat ring are also present in a nominally flat ring with misalignments.

In a nominally flat HERA ring with random misalignments within the alignment specifications and after the orbit has been corrected by conventional methods with correction coils, the rms tilt $|\delta \boldsymbol{n}_0|$ of the periodic axis from the vertical can be typically 30 mrad. Simulations suggest that after the conventional closed orbit correction, the strongest component of spin diffusion is that due to the tilt of the $\hat{n}_0$ axis combined with the large horizontal orbital oscillations. The vertical misalignment of the quadrupoles which causes the tilt cannot be easily controlled. The spin matching conditions, applicable in the case of a few vertical bends, cannot be applied to correct for the random misalignments of hundreds of quadrupoles. But closed orbit corrections utilizing a small set of vertical correction coils can be used to generate additional controlled tilts and thereby reduce the rms tilt and hence reduce spin diffusion.

In summary, spin diffusion can be a very strong effect (relative to the Sokolov–Ternov effect) in a real storage ring, and in order to achieve a high degree of polarization, it is necessary to minimize it. If the ring is not flat, as in the case of HERA with spin rotators, then the optic can be optimized using the technique of spin matching. The magnets in the ring should be well aligned, and the vertical dispersion caused by the misalignments can be minimized with conventional closed orbit corrections. After these steps, the maximum polarization may still be reduced by the spin diffusion resulting from the tilt of $\hat{n}_0$ from the design direction, caused by the horizontal magnetic fields on the closed orbit. The correction of this tilt requires a special orbit correction scheme, an example of which is described in the next section.

2.2. Correction of the $\hat{n}_0$ tilt

The method used at HERA to correct the tilt is based on the formalism described in refs. [14,15] and the correction scheme is described in ref. [16]. General features of the algorithm are described here, for completeness. An earlier, less general formalism is described in ref. [17].

The "design" closed orbit of a storage ring is defined on the basis of the design positions of the magnets. The "actual" closed orbit of an imperfect storage ring is determined by the misalignments of the magnets and the fields of the correction coils; the distortions of the design field on the design closed orbit are denoted by $\Delta \boldsymbol{B}(s)$. For small perturbing fields $\Delta \boldsymbol{B}$, one can write the difference $\delta \boldsymbol{n}_0$ between the unit periodic solutions $\hat{n}_0$ of the Thomas–BMT equation along the actual and the design closed orbits in the form

$$\delta \boldsymbol{n}_0 = \alpha \hat{\boldsymbol{m}}_0 + \beta \hat{\boldsymbol{l}}_0, \tag{8}$$

with $|\alpha| \ll 1$ and $|\beta| \ll 1$; $\hat{\boldsymbol{m}}_0$ and $\hat{\boldsymbol{l}}_0$ are (in general non periodic) solutions of the Thomas–BMT equation along the design orbit, chosen to form together with $\hat{n}_0$ a right-handed orthonormal basis. $\delta \boldsymbol{n}_0$ is periodic, so it is convenient to describe it in a periodic basis. This is

done by introducing the vectors $\hat{\boldsymbol{m}}$ and $\hat{\boldsymbol{l}}$, related to $\hat{\boldsymbol{m}}_0$ and $\hat{\boldsymbol{l}}_0$ by

$$[\hat{\boldsymbol{m}} + \mathrm{i}\hat{\boldsymbol{l}}](s) = \mathrm{e}^{-\mathrm{i}\psi(s)}\left[\hat{\boldsymbol{m}}_0 + \mathrm{i}\hat{\boldsymbol{l}}_0\right](s), \tag{9}$$

where ψ is chosen so that

$$\psi(s + C) = \psi(s) + 2\pi(\nu + k),$$

with C being the circumference of the ring and k being any integer. For HERA, k and ψ are chosen such that $\psi(s) = 2\pi\tilde{\nu}s/C$, where $\tilde{\nu}$ is the fractional part of the spin tune, with the phase ψ set to zero at the East IP.

Using the periodic basis and describing the coupling of the spin motion to the orbital motion in linear approximation, one finds for α and β the following Fourier expansion

$$(\alpha - \mathrm{i}\beta)(s) = -\mathrm{i}\frac{C}{2\pi}\sum_k \frac{f_k}{k - \tilde{\nu}}\mathrm{e}^{\mathrm{i}2\pi k s/C}. \tag{10}$$

The f_k are the Fourier components of a "spin–orbit function" $f(s) \equiv [f_{\mathrm{Re}} - \mathrm{i}f_{\mathrm{Im}}](s)$ which is a linear function of the closed orbit and the perturbing fields $\Delta\boldsymbol{B}$ [15]:

$$\begin{pmatrix} f_{\mathrm{Re}} \\ f_{\mathrm{Im}} \end{pmatrix} = \mathbf{L}\left[\mathbf{F}\boldsymbol{x} - \frac{e}{E_0}\begin{pmatrix} \Delta B_s(1+a) \\ \Delta B_x(1+a\gamma) \\ \Delta B_y(1+a\gamma) \end{pmatrix}\right], \tag{11}$$

where e is the unit electric charge, E_0 is the beam energy, $\mathbf{L}$ is a 2×3 matrix containing the components of $\hat{\boldsymbol{m}}$ and $\hat{\boldsymbol{l}}$ in the orbital reference system, $\mathbf{F}$ is a 3×6 (energy dependent) matrix containing the nominal fields and gradients, $\boldsymbol{x}$ is the actual 6-dimensional closed orbit, and ΔB_s, ΔB_x, ΔB_y are the longitudinal, horizontal, and vertical components of $\Delta\boldsymbol{B}$.

For the common case of a machine without rotators, solenoids and skew quadrupoles, the dominant source of the tilt is the distortion of the closed orbit y_{co} caused by the vertical misalignments of the quadrupoles, and the spin–orbit function f takes the simple form

$$f(s) = -(1 + a\gamma)\,\mathrm{e}^{\mathrm{i}[\psi(s) - \nu\phi_{\mathrm{B}}(s)]}y''_{\mathrm{co}}, \tag{12}$$

where y''_{co} is the second derivative of the vertical closed orbit and ϕ_{B} is the cumulative bending angle. Thus in this formalism, $f(s)$ for these machines is simply related to y''_{co} (see also ref. [17]).

The principle of the harmonic spin–orbit correction scheme is to make additional orbit corrections using vertical correction magnets, and reduce the rms tilt by changing and minimizing the Fourier coefficients f_k in a controlled manner. Under the assumption that the tilt is dominated by the components f_k for k near $\tilde{\nu}$, the depolarizing effects due to misalignments can be reduced by canceling only a few harmonics; from eq. (10) one can see that $\delta\boldsymbol{n}_0$ is sensitive in particular to the spin–orbit harmonics with k equal to 0 and 1. Important criteria for selecting an orbit adjustment scheme for generating the correction harmonics include the following:

- Maximum tilt correction with minimum distortion of the original closed orbit. Large orbit deviations in sextupoles increase the vertical dispersion, which itself is a source of spin diffusion through the resulting vertical orbital oscillations. Thus if the orbit distortions required for the spin–orbit correction are large then the effect of the tilt correction may be spoiled by increasing the spin diffusion from other sources.
- Orthogonality of the components, to allow an independent adjustment of the amplitude of each harmonic.
- Minimum orbit deviation at the electron–proton interaction points (IP) and the electron–laser beam IP of the polarimeter. Changes of the correction amplitudes can then be made without interruption of the luminosity operation of the collider and of the polarization measurement.
- Applicability of the correction scheme for general distributions of misalignments and orbit errors.
- Successful increase of the polarization also when higher order effects are included.

The first harmonic spin–orbit correction scheme to be applied to an electron storage ring was that developed for PETRA [17]. The same scheme has also been used more recently at TRISTAN [18]. That orbit adjustment algorithm is based on the adjustment of individual vertical correction coils distributed around the ring, and is restricted to the case where $\hat{\boldsymbol{n}}_0$ is nominally vertical everywhere. In contrast, the formalism described here is designed to be able to handle a nominally non-flat machine, and simulations indicate that it is more successful in the compensation of the misalignments in HERA with spin rotators installed [19].

2.3. The implementation at HERA

Simulations have shown that the harmonics -1, 0, 1 and 2 of f must be controlled; each harmonic has a real and an imaginary part so that eight real components $\tilde{f}_i$, $i = 1, 2, \ldots, 8$ must be generated. This is done by perturbing the vertical closed orbit using vertical correction coils. In order to not perturb the orbit everywhere, the eight components are generated using a "family" of eight closed orbit bumps located in the arcs of the ring. The periodic magnet lattice in the HERA arcs is shown in Fig. 1 together with the geometry of a single closed orbit bump. A bump is created using three consecutive vertical correction coils: the first deflects the beam from the original closed orbit, the second returns it to the position of the original orbit at the location of the third coil, which finally compensates the residual angle. The vertical dispersion

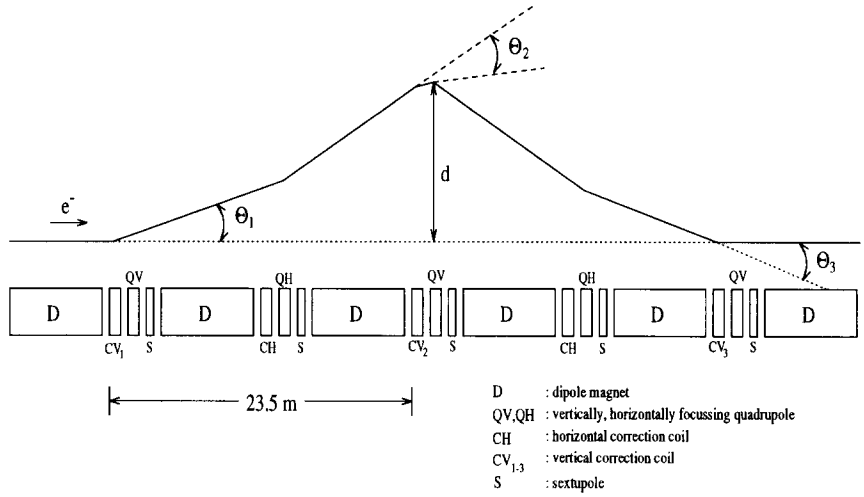

Fig. 1. The periodic magnet lattice in the HERA arcs. A single "FODO cell" contains two dipole magnets, two quadrupoles, two sextupoles, and two correction coils. The length of one cell is 23.5 m, and the phase advance of the betatron oscillations is 60° per cell. Also shown is a schematic drawing of a vertical closed orbit bump utilizing three consecutive vertical correction coils. The first coil produces a kick θ_1 and the subsequent coils produce kicks $\theta_2 \approx -\theta_1$ and $\theta_3 = \theta_1$; the kicks produced by the quadrupoles are also indicated. The maximum orbit deviation is denoted by d. The total length of a bump is 47.0 m.

generated by the bump because the beam is off-center in the sextupoles is estimated to be small.

The amplitudes of the generated components $\tilde{f}_i$ depend linearly on the strengths of the 24 kicks θ_i, and the problem is described by the simple matrix equation

$$\mathbf{M}\boldsymbol{\theta} = \tilde{\mathbf{f}}, \tag{13}$$

where $\mathbf{M}$ is an 8×24 matrix; see ref. [15] for its functional form. Since the magnitudes of the second two kicks of each bump are dictated by the magnitude of the first by the constraint that the bump must be closed, $\mathbf{M}$ can be reduced to an 8×8 matrix and, instead of specifying the amplitude of the bump with the strength of the "leading" kick, one can use the maximum orbit deviation d (see Fig. 1). This leads to a new matrix equation

$$\bar{\mathbf{M}}\mathbf{d} = \tilde{\mathbf{f}}. \tag{14}$$

If $\bar{\mathbf{M}}$ is nonsingular, the required correction amplitudes $\mathbf{d}$ can be computed from $\tilde{\mathbf{f}}$ by inversion. The computation of the matrix $\bar{\mathbf{M}}$ and of its inverse is done by a modified version of the computer program FIDO [20].

The ring contains a total of 200 vertical correction coils in the arcs; one can use several algorithms to organize them into families of eight bumps. The determinant of the corresponding matrix $\bar{\mathbf{M}}$ is used as an estimate of the effectiveness of a family: a large value of $\det(\bar{\mathbf{M}})$ implies a large corrective strength with minimum orbit deviation. A selected family is optimum over an energy range of about ± 0.5 GeV. It has been found that the best results are obtained by using the arrangement shown in Fig. 2, similar to the symmetry of the scheme adopted at PETRA. Two bumps are positioned in each arc, each a distance S from the center of the arc. This arrangement is mirror-symmetric across the diameters through the IPs and through

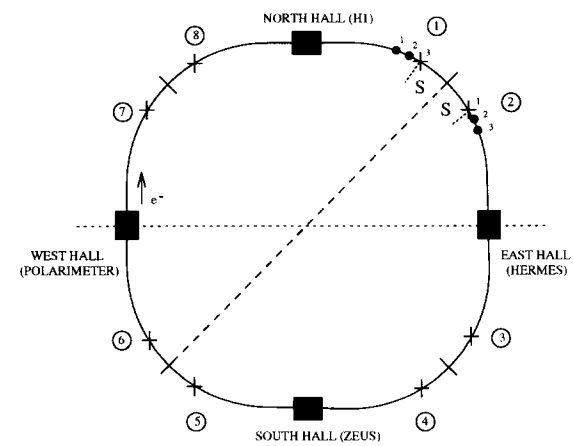

Fig. 2. A schematic drawing of the HERA ring showing the arrangement of the eight closed orbit bumps (numbered 1 through 8). The positions of the three coils (see Fig. 1) of bumps 1 and 2 are also shown. The distance S is the distance from the center of the arc to the nearest coil in the bump. The arrangement is mirror-symmetric across diameters through the IPs and the mid-points of the arcs; two of the lines-of-symmetry are drawn. The optimum distance S was determined to be 119 m; the length of one octant is 792 m.

the mid-points of the arcs. The family with the maximum determinant at 26.7 GeV was obtained with the distance $S = 119$ m.

The equilibrium polarization is sensitive to the actual misalignments and field errors in the ring, and to the correction fields used to minimize the resulting rms distortion of the closed orbit. The residual systematic errors in the positions of the magnets and of the beam position monitors make it difficult to precisely determine the fields on the closed orbit. Thus, in practice, it may not be possible to accurately predict the amplitudes $\boldsymbol{d}$ of the eight bumps needed to correct the $\hat{\boldsymbol{n}}_0$ tilt caused by the field distortions. In this case there are two important consequences: firstly, the optimum amplitudes of the corrections must be determined empirically. Thus an extended programme, guided by a fast polarimeter, of measurements of the polarization as a function of each of the eight correction amplitudes is required to perform the tilt correction. If the systematic errors in the orbit position monitors were sufficiently small then it would be possible to use this information to speed-up the optimization process; this application of the orbit measurements at HERA is under study. Secondly, the effectiveness of the family of bumps chosen for maximum det($\overline{\mathbf{M}}$) must be studied to determine if the correction of all eight spin-orbit harmonics using the selected family is sufficient to improve the polarization under a variety of misalignment conditions (i.e. for a variety of different closed orbits). The results of these simulations are discussed in the following section.

2.4. Simulations of the optimization procedure

In order to simulate the diffusion processes of a "typical" ring, it is necessary to include the misalignments and field errors of the magnets of the ring and also the correction fields used to reduce the rms closed orbit distortions. The misalignments are taken from Gaussian distributions with rms widths given by the measured distributions. Conventional closed orbit corrections can then be simulated in order to achieve a realistic value of the rms distortion of the vertical closed orbit of about 0.7 mm. The effect of the $\hat{\boldsymbol{n}}_0$ axis tilt correction on the polarization is then investigated. The optimization is performed by varying one component while keeping the other seven unchanged. The relative amplitudes of the 8 bumps which characterize each spin–orbit component are given by the columns of the inverse of $\overline{\mathbf{M}}$. The strength of a component is measured by the amplitude of the bump with the largest relative orbit deviation, denoted by D. The optimum amplitude of a component is denoted by D_{opt}.

An example of the optimization procedure is shown in Fig. 3. The equilibrium polarization $P_{\max}$ is plotted as a function of the amplitudes D of the harmonics 0 and +1, for a "typical" HERA ring. The polarization is seen to be a strong function of the amplitudes, and for the particular error distribution simulated, the components 0-Imaginary and +1-Real can be used to significantly increase the polarization whereas only a small improvement is possible using the 0-Real and +1-Imaginary components. The effect of the −1 and +2 harmonics is significantly weaker than that of the 0 and +1 harmonics. Before correction, the rms tilt $|\delta \boldsymbol{n}_0|$ is 19.4 mrad, and the equilibrium polarization is 27.1%; with each of the 8 harmonic components set to its corresponding D_{opt}, the rms tilt is reduced to 12.5 mrad and $P_{\max}$ is 81.0%. On the basis of such studies, an equilibrium polarization $P_{\max}$ after corrections of between 60 and 80% is achievable utilizing the family selected for use at 26.7 GeV, and the maximum required total orbit deviation is about 5 mm.

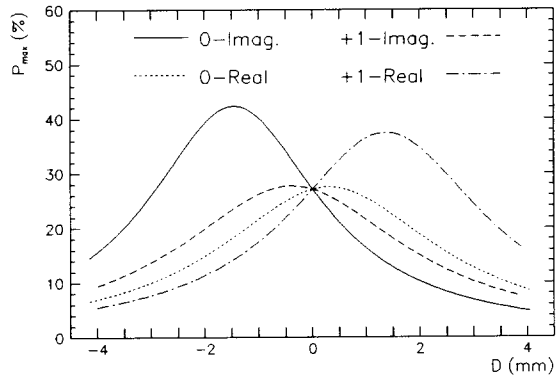

Fig. 3. The asymptotic polarization $P_{\max}$ plotted as a function of the amplitudes D of the components of the 0 and +1 harmonics. In this simulation the 0-Imaginary and +1-Real components are found to significantly increase the polarization; in this case the required values, D_{opt}, for the components are −1.4 and 1.3 mm, respectively. The value of the polarization is less sensitive to the amplitudes of the −1 and +2 harmonics. The maximum polarization is increased from 27.1% to 81.0% when the eight amplitudes are put to their optimum settings. The simulations are made in the linear approximation [5], and thus include the effects of only first order resonances.

It is important to point out differences between the actual and the simulated optimization procedures. In Fig. 3 we have plotted the equilibrium polarization $P_{\max}$, but in practice one measures a polarization $P(t)$ which may be varying in time as it approaches equilibrium. Thus small increases in the equilibrium polarization due to the corrections may be difficult to measure. In addition, the tilt $|\delta \boldsymbol{n}_0|$ is a linear function (10) of the magnitudes of the harmonics, but the polarization is a non-linear function of the tilt. It is then possible that the tilt correction of a particular harmonic component

may have a negligible effect on the polarization when the polarization is small, but a more noticeable effect when the polarization level is greater. Thus a sensitive measurement of the optimum amplitudes may require that the corrections are iterated. The eight components are, to a good approximation [#2], orthogonal and so can be individually optimized and combined to achieve the maximum polarization.

Next we discuss an example of the effect of the corrections on the energy dependence of the polarization. In figs. 4a and 4b we show results for the equilibrium polarization obtained from Monte Carlo simulations using SITROS. A single "typical" HERA machine with misalignments and conventional closed orbit corrections has been simulated; the equilibrium polarization is shown before and after the optimization of the harmonic corrections. The energy dependence of the polarization and the resonance structure are discussed in more detail in section 7. As shown in Fig. 4a the maximum polarization, after conventional orbit corrections are performed, is 23%. The optimization using the harmonic corrections increases the maximum polarization to 70%. The increase is predicted by both the linear and non-linear simulations, showing that as expected, the spin diffusion of the higher order resonances is also reduced by the tilt correction.

The simulation of a single "typical" HERA machine is useful for predicting the *tendencies* for relative strengths of resonances. Because the actual polarization depends very strongly on the precise error distribution, a *prediction* for the expected polarization based on the specifications for the alignment of the magnets and realistic closed orbit corrections can be obtained only from an average of the results from many "typically" misaligned rings. Such a study has been performed with SITROS on four different rings; the average maximum polarization before optimization of the harmonic corrections is $26.0 \pm 6.0\%$, and the maximum is increased by the corrections to $70.7 \pm 6.7\%$.

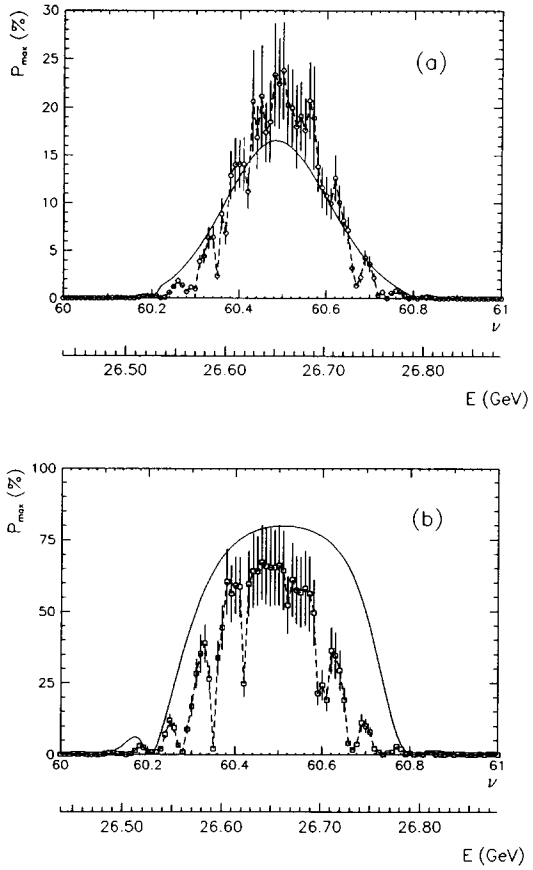

Fig. 4. Results of Monte Carlo simulations of the polarization as a function of the beam energy and of the spin tune ν, between two integer resonances for a "typical" HERA ring. The results of linear calculations (solid curves) are shown for comparison. The maximum polarization attained after simulating conventional orbit corrections, shown in (a), is about 23%. The effect of the harmonic corrections is shown in (b), with the polarization reaching 70%. The error bars represent the statistical error of the Monte Carlo simulations; the spin diffusion is simulated by tracking 50 particles for 5000 orbits around the ring, corresponding to 0.11 s or 13 times the damping time constant of the energy oscillations. The strength of the synchrotron sidebands can be underestimated by the Monte Carlo simulations in the case of strong depolarization. This effect is dependent on the sampling of the tails of the non-Gaussian particle distributions, and is visible in the results shown in (a), where the polarization, with the effects of the higher order sidebands included, is estimated to be slightly higher than the linear result.

3. The HERA polarimeter

The vertical component of the electron polarization is measured using the asymmetry of the Compton cross section for scattering of vertically polarized electrons off circularly polarized photons [21]. Laser light of 514 nm is directed against the electron beam and the energy E_γ and vertical position y of the backscattered photons are measured. The polarization P_y is obtained from the difference Δy in the mean vertical positions $\langle y \rangle$ of the distributions measured with left and right circularly polarized light:

$$\Delta y(E_\gamma) = \frac{\langle y \rangle_L - \langle y \rangle_R}{2} \tag{15}$$

$$= P_y \frac{S_{3,L} - S_{3,R}}{2} \Pi_y(E_\gamma)$$

$$= P_y \Delta S_3 \Pi_y(E_\gamma), \tag{16}$$

[#2] Neglecting nonlinear (sextupole) fields and deviations of the quadrupole fields from the design values.

$$= P_y \Delta S_3 \Pi_y(E_\gamma), \tag{16}$$

where $S_{3,L}$ and $S_{3,R}$ are the degrees of circular polarization of the laser light and $\Pi_y(E_\gamma)$, the analyzing power, is derived from the polarization dependent Compton cross section, as explained in ref. [2]. The maximum value of $\Pi_y(E_\gamma)$ is 180 μm at $E_\gamma = 8.0$ GeV. In practice ΔS_3 is nearly 1, and the vertical component of the electron beam polarization P_y is proportional to Δy. A detailed analysis of the 2-dimensional scattering distributions has been performed in order to estimate the systematic errors in the measurement [2].

The HERA polarimeter has been described in detail in ref. [2]. The major components are briefly described here together with the modifications made since 1991 which influence the systematic errors of the polarization measurement.

3.1. The calorimeter

The energy and vertical position of the backscattered photons are measured using a tungsten-scintillator sampling calorimeter [22,23]. The calorimeter is horizontally split in the middle, and can thus be considered to consist of two calorimeters, one on top of the other. The energy of an incoming photon is the sum of the energies in the two halves:

$$E_\gamma = E_{\text{up}} + E_{\text{down}}, \tag{17}$$

and the vertical position is measured using the asymmetry of the energies:

$$\eta(y) = \frac{E_{\text{up}} - E_{\text{down}}}{E_{\text{up}} + E_{\text{down}}}. \tag{18}$$

The transformation function $\eta(y)$ is related to the average transverse distribution of the energy deposition of an electromagnetic shower in the calorimeter dE/dy by

$$\eta(y) = 1 - \int_{-\infty}^{-y} \frac{dE}{dy'} dy', \tag{19}$$

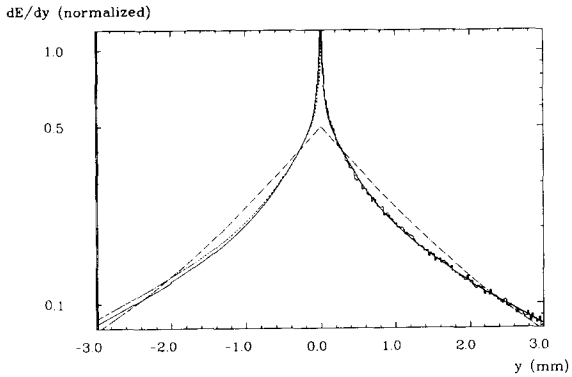

Fig. 5. The normalized shower distribution dE/dy derived from test beam measurements (dashed curve) and the parametrization of the EGS4 results (solid curve). Also shown for comparison are the results of the EGS4 simulation ($y > 0$; histogram) and the optimized parametrization ($y < 0$; dotted curve). Note the very narrow component of the shower near $y = 0$, not seen in the test beam results, which was necessary to achieve the good agreement of the measured and predicted $dN/d\eta$ distributions (Fig. 6).

with the normalization condition (assuming cylindrical symmetry of the energy deposition)

$$\int_0^\infty \frac{dE}{dy'} dy' = 1. \tag{20}$$

The simulations of $dN/d\eta$ described in ref. [2] utilized an $\eta(y)$ transformation derived from test beam measurements [22]. But difficulties were found in achieving a good fit to the measured vertical distributions using this transformation, therefore simulations of the shower development in the calorimeter using the Monte Carlo program EGS4 [24] have been utilized to derive a parametrization of eq. (19). The parameter values were optimized by fitting the measured $dN/d\eta$ distributions [25]. The distribution of the transverse energy deposi-

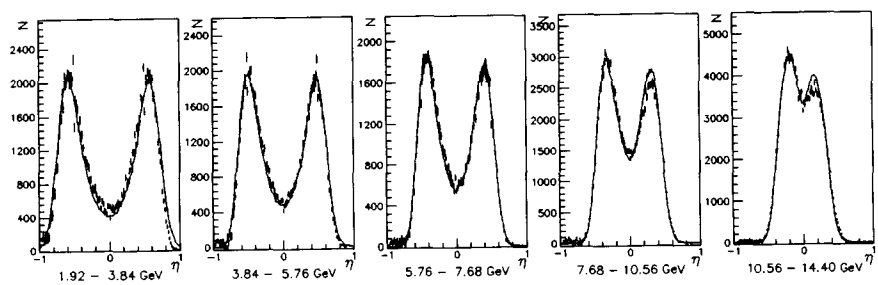

Fig. 6. The measured vertical distributions $dN/d\eta$ of the backscattered photons with the background subtracted, shown in five energy intervals. The endpoints of the intervals are indicated below the figures. The predicted distributions (overlaid) have been calculated with a Monte Carlo program which utilizes the Compton differential cross section and the optimized $\eta(y)$ parametrization, and includes the effects of the calorimeter energy and position resolution and the electron beam divergence. The agreement is satisfactory and much improved compared to ref. [2], Fig. 23.

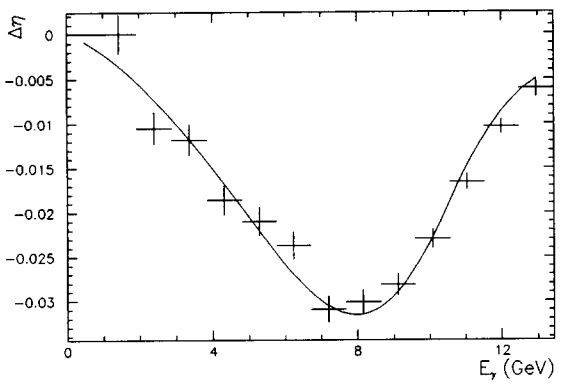

Fig. 7. The polarization measurement for a typical run: $\Delta\eta$ is plotted as a function of E_γ. The fit to eq. (22) (solid curve) gives $\Delta S_3 P_y = 53.1 \pm 1.0\%$.

tion dE/dy determined from the test beam measurements, the EGS4 simulations, and the optimization of the EGS4 parametrization are compared in Fig. 5. The good agreement of the measured $dN/d\eta$ distributions and the predictions made utilizing the optimized $\eta(y)$ parametrization can be seen in Fig. 6.

The polarization P_y can be obtained from the difference of the mean vertical positions $\langle\eta\rangle$ measured with right and left circularly polarized light (compare with eqs. (15) and (16)):

$$\Delta\eta(E_\gamma) = \frac{\langle\eta\rangle_L - \langle\eta\rangle_R}{2} \tag{21}$$

$$= P_y \Delta S_3 \Pi_\eta(E_\gamma). \tag{22}$$

The analyzing power $\Pi_\eta(E_\gamma)$ has been derived using the optimized $\eta(y)$ transformation. The measured difference $\Delta\eta(E_\gamma)$ in a typical run is shown in Fig. 7, together with the result of the fit to eq. (22). The agreement is excellent. For $\Delta S_3 = 1$, the value of the vertical polarization P_y from the fit is $53.1 \pm 1.0\%$, with the $\chi^2/\text{ndf} = 1.1$. The average analyzing power in the energy interval $5.4 < E_\gamma < 11.7$ GeV (the range used in the calculation of on-line results) calculated with the optimized $\eta(y)$ transformation is 0.0493, compared with the previous value of 0.0456.

The vertical polarization can also be obtained from measurements of the asymmetry $\mathscr{A}(\eta, E_\gamma)$ derived from the 2-dimensional distributions $N_{L,R}(\eta, E_\gamma)$:

$$\mathscr{A}(\eta, E_\gamma) = \frac{N_L(\eta, E_\gamma) - N_R(\eta, E_\gamma)}{N_L(\eta, E_\gamma) + N_R(\eta, E_\gamma)} \tag{23}$$

$$= \Delta S_1 \Sigma'_{1/0} + \Delta S_3 P_y \Sigma_{2Y/0}, \tag{24}$$

where $N_{L,R}(\eta, E_\gamma)$ are the number of scattered photons at the vertical position η in the energy interval between E_γ and $E_\gamma + \Delta E_\gamma$, measured with left and right circularly polarized light. The definitions of the functions $\Sigma'_{1/0}$ and $\Sigma_{2Y/0}$ can be found in ref. [2]. The data are fit to eq. (24) with $\Delta S_3 P_y$ and ΔS_1 (the difference between the linear polarization components $S_1(0)$ of the left and right polarized beams [2]) as free parameters. Shown in Fig. 8 are the measured asymmetry distributions, $\mathscr{A}(\eta, E_\gamma)$, in the five energy intervals defined in Fig. 6. The fit results are overlaid in the figure. The agreement of the predicted and measured curves is excellent. The fit yields $\Delta S_3 P_y = 0.548 \pm 0.007$ and $\Delta S_1 = 0.088 \pm 0.004$. The value of $\Delta S_3 P_y$ is consistent with that obtained in the fit to $\eta(E_\gamma)$, shown in Fig. 7.

3.2. The path of the backscattered photons

The backscattered photons leave the electron ring vacuum pipe through an aluminum window 29 m from

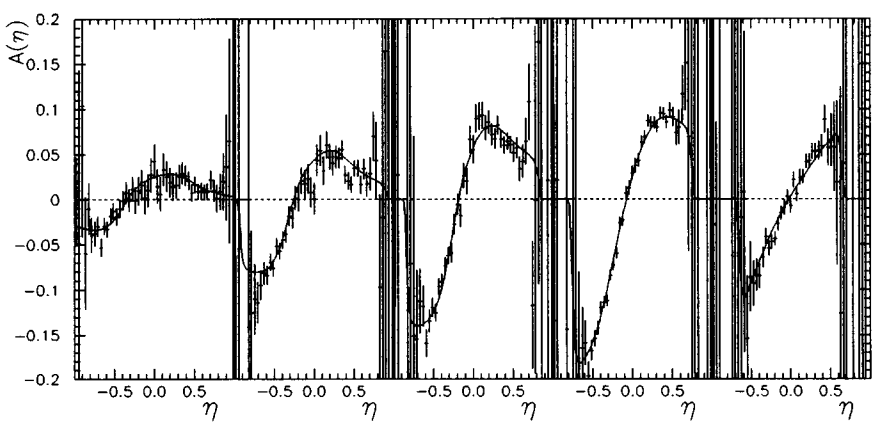

Fig. 8. The asymmetry distributions $\mathscr{A}(\eta)$ calculated in the five energy intervals, ΔE_γ, defined in Fig. 6. The data are the same as used for Fig. 7. The simultaneous fit to eq. (24) in the five intervals gives $\Delta S_3 P_y = 0.548 \pm 0.007$, in excellent agreement with the results of the fit to eq. (22). The effective linear component of the laser light $\Delta S_1 = 0.088 \pm 0.004$.

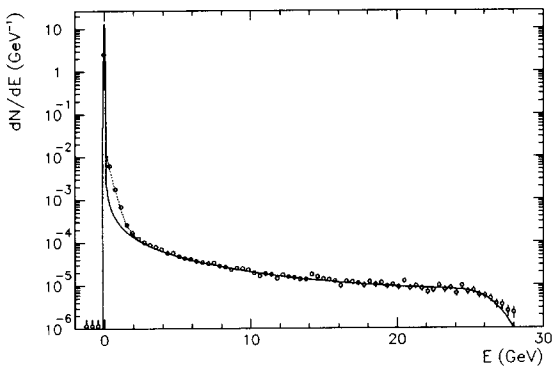

Fig. 9. The energy spectrum of the background measured for a bunch current of 0.28 mA at 26.7 GeV. The predicted spectrum of beam–gas bremsstrahlung corresponding to a vacuum pressure of 1.6×10^{-9} mbar is overlaid (solid curve). The predicted energy spectrum including the Compton scattered blackbody photons, corresponding to a temperature of 310 K, is also shown (dotted curve) [26]. A calorimeter energy resolution of $\sigma_E = 24\%\ \sqrt{E(\mathrm{GeV})}$ was assumed in the calculations.

the IP and travel 36 m to the detector. Collimators and sweeping magnets are used to remove background. There is a 10% probability for conversion in the air between the exit window and the detector. The degraded measurement of the energy and position of converted photons results in long tails in the vertical distributions and distortions of the characteristic energy spectra of bremsstrahlung and of the Compton scattered photons. These effects were seen in the November 1991 data. The path is now evacuated (except for a section of 9 m) and the conversion probability is reduced to about 3%. The tails of the vertical distributions are now negligible (see Fig. 6), and the energy distributions are in excellent agreement with the predictions. As an example, the background spectrum at a beam energy of 26.7 GeV, measured with the laser beam blocked, is shown in Fig. 9. The agreement with the Bethe–Heitler prediction is excellent except at low energies where the background is dominated by the scattering of the electrons on the blackbody (thermal) photons in the chamber. The deviation is in good agreement with the expected contribution for a temperature of 310 K [26].

3.3. The polarization of the laser light

A continuous beam of laser light (10 W, 2.41 eV) is scattered on the electron beam. The transport system is described in detail in ref. [27]; only the components relevant for the light polarization are described here. The light is directed over the 180 m from the laser laboratory to the electron vacuum chamber with high reflectivity dielectric mirrors. No optical components are inside the electron ring vacuum, thus the light must enter the vacuum chamber nearly (anti)parallel to the electron beam direction, and great care had to be taken with the installation of the vacuum windows to minimize their influence on the polarization of the laser light.

The polarization is switched between vertical linear polarization and left and right circular polarizations using a Pockels cell. The Pockels cell voltages are optimized on the basis of measurements with the polarization analyzer located after the exit window. Measurements in spring 1992 indicated that the vacuum windows were birefringent, with a net phase shift of the vertical polarization component relative to the horizontal of approximately $\lambda/12$. The effective linearly polarized component in the laser light at the IP can be measured from the backscattered distributions [2], and the results were consistent with the analyzer measurements. Thus only the entrance window was birefringent and the values given by the analyzer corresponded to the polarization of the laser light at the IP. Circular polarizations S_3 greater than 99% at the IP could be achieved. Measurements of the backscattered distributions in the summer and fall of 1992 indicated an increase of the linearly polarized component at the IP, in disagreement with the analyzer results. This indicated that the exit window had also become slightly birefringent. We estimate that the value of ΔS_3 was between 0.90 and 0.99. The birefringence was not observed in measurements taken at the end of the run period, in November 1992. The cause of the birefringence appears to be stresses in the glass caused by the window mounts, and the stresses appear to be sensitive to the history of the vacuum of the electron ring.

4. The machine conditions and the data collected

The measurements have been made at beam energies near 26.67 GeV, corresponding to a half-integer spin tune of 60.5, as in November 1991. As noted in section 1, the optic of the electron ring used for luminosity operation was modified for the polarization studies by reducing the horizontal and vertical betatron tunes, Q_x and Q_y, from 47.22 and 47.35, to 47.12 and 47.20, respectively. This moves the energies of the linear betatron resonances closer to the integer resonances, increasing the energy separation of the resonances and potentially increasing the polarization near half-integer spin tunes. The strengths of the synchrotron sideband resonances are expected to decrease with increasing synchrotron tune. Thus the ring was operated with the maximum available total circumferential voltage of about 160 MV, profiting from the superconducting cavities installed in the electron ring

[28]. During the measurements, the voltage ranged between 140 and 165 MV. The measured synchrotron frequency ranged between 2.9 and 3.9 kHz, corresponding to synchrotron tunes Q_s between 0.061 and 0.082. This choice of tunes satisfies $Q_y = Q_x + Q_s$, which puts the families of synchrotron sidebands of the parent betatron resonances on top of each other. The orbit of the ring is stable and reproducible over many shifts, thus special correction of the orbit before the polarization measurements was not needed. The rms distortion of the vertical closed orbit achieved with the conventional orbit corrections was between 0.7 and 0.8 mm. The electron ring was operated in stand-alone mode: the solenoids and compensators of the ZEUS and H1 detectors were not powered, nor was the proton ring.

The polarization was measured in a 1 min cycle consisting of 40 s of Compton scattering measurements while switching the laser polarization between left and right circular polarizations at 90 Hz, followed by 20 s of background measurements with the laser beam blocked. The total electron current had been limited to about 2 mA distributed over ten bunches and having a beam lifetime of about 5 h. Under these conditions about 3500 scattered photons with $E_\gamma > 1.8$ GeV were recorded in a 1 min measurement, giving a statistical error ΔP_y of about ± 0.03.

The main objective of the measurements during 1992 was to maximize the electron polarization. As the energy scale of the ring is uncertain to ± 50 MeV, scans of the polarization versus the beam energy were made (section 7) to find the optimum energy at which to begin the correction studies. After fixing the energy, a scan of the RF voltage was made to insure that the operating energy was not near the position of a synchrotron sideband resonance. The maximum polarization achieved at this stage was 25.5% at 26.700 GeV, compared to 8% in November 1991. After these preparatory measurements the effects of the 0 and +1 spin–orbit harmonics were studied, followed by the harmonics −1 and +2. The effect of the correction of the tilt of the electron beam ellipse was also measured. These studies are discussed in the next section.

Other polarization studies were also performed. The longitudinal component of the polarization P_z was monitored, and was consistently zero during the studies within the statistical error (± 0.01). The build-up time τ was measured and used to check the systematic error in the polarization scale. The results indicate that the systematic error in the scale is less than the statisti-

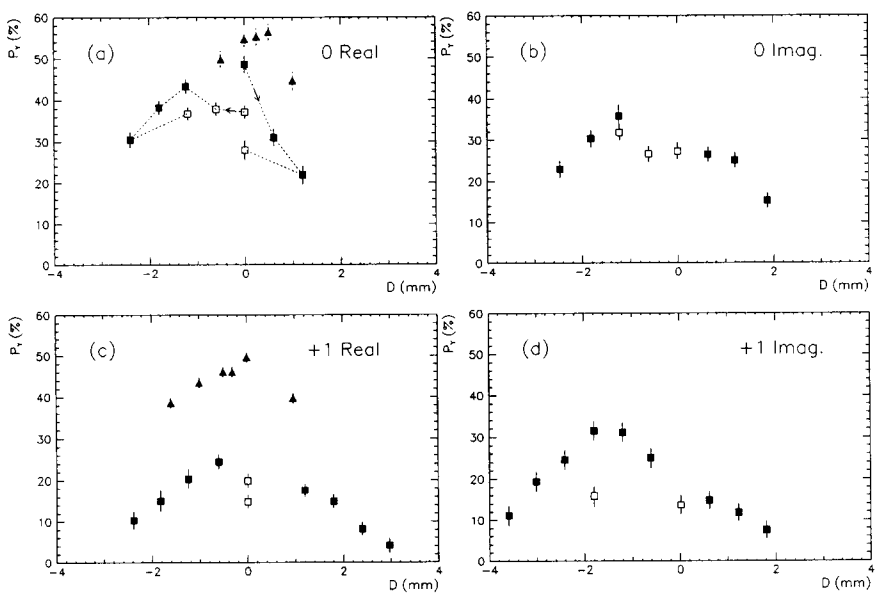

Fig. 10. Studies of the four main components of the harmonic spin–orbit corrections: 0-Real and 0-Imaginary; +1-Real and +1-Imaginary. The measured polarizations are plotted versus the component amplitudes D (the maximum of the orbit deviations in the eight bumps). Measurements are collected which were performed under constant conditions; for 0-Real and +1-Real a second scan is shown (△) which was performed to check the first result. Open symbols are used to indicate values which are believed to be too low with respect to neighboring points because of build-up time effects. The measurements comprising the two parts of the first scan of 0-Real are connected: the scan began at 0 mm, with a polarization of $48.6 \pm 2.0\%$, and positive amplitudes were checked. The scan was continued, following loss of the beam, with measurements at negative amplitudes; see also Fig. 11. The optimal amplitudes D_{opt} are found to be 0 mm for 0-Real and +1-Real; −1.2 mm for 0-Imaginary and −1.8 mm for +1-Imaginary. The systematic error ΔD_{opt} is estimated to be ± 0.5 mm for these components.

cal error of the measurement ($\pm 0.10\ P_y$), thus we have continued to use the polarization scale described in ref. [2]; this point is described in more detail in section 6. The dependence of the polarization on the beam energy was measured in five short energy scans.

5. Orbit correction studies

5.1. Harmonic spin–orbit corrections

As described in section 2.2, the harmonic spin-orbit corrections are specifically designed for increasing the polarization. The optimum amplitudes for the corrections could not be precisely predicted by orbit measurements, and therefore were determined empirically, guided by the on-line results of the polarimeter. The 8 amplitudes, $\boldsymbol{D}_{\rm opt}$, can be determined by measuring $P_{\rm max}$ as a function of the component amplitudes D, as plotted in Fig. 3. The asymptotic values $P_{\rm max}$ can be measured at each point by depolarizing and measuring the build-up time (section 6), but this requires a lot of beam time. In practice, the points were measured by waiting typically between 5 and 25 min (decided by the person(s) on shift) at each amplitude, and recording the average polarization in the last five minutes of the measurement. The largest source of error in the measurement of the $\boldsymbol{D}_{\rm opt}$ is the systematic error due to the short measurement times and the long build-up time τ; this effect is discussed in the following section.

The harmonics 0 and +1 are expected to have the strongest effect on the polarization; selected results of the measurements of these four corrections are shown in Figs. 10a–d. The four components all strongly affected the polarization, and the measurements are in qualitative agreement, with respect to the shape of the curves and the characteristic amplitudes of about 2 mm, with the curves shown in Fig. 3. For the real parts the maximum polarization was obtained with the amplitudes at zero and thus these components did not increase the polarization. The corresponding values for $\boldsymbol{D}_{\rm opt}$ are equal to zero. The imaginary components exhibited the desired effect: the maximum polarization was found at non-zero amplitudes, indicating that the orbit corrections had successfully cancelled the contributions to the spin–orbit function f caused by the alignment errors. The optimum amplitude $\boldsymbol{D}_{\rm opt}$ of 0-Imaginary was found to be -1.2 mm and of +1-Imaginary to be -1.8 mm. The harmonics -1 and +2 were studied with polarizations of approximately 50%, and the effect of the corrections was very small over a range in amplitudes of ± 2 mm; the corresponding measured values for $\boldsymbol{D}_{\rm opt}$ are zero.

5.1.1. Systematic errors from the build-up time

As mentioned above, the dependence of the asymptotic polarization $P_{\rm max}$ on the amplitudes $\boldsymbol{D}$ of the harmonic components was measured by changing the amplitudes and recording the polarization after waiting for some time, until the value appeared to be stable within the statistical error as judged by the person(s) on shift. If the amplitude of a correction is changed too frequently, then the recorded polarizations may differ from $P_{\rm max}$, at each point, by more than the statistical error of the measurement. A long build-up time can thus introduce a systematic error in the measurement of $P_{\rm max}$ which is much larger than the statistical error, and the magnitude of this error depends on the value of $P_{\rm max}$, the value of the polarization when the amplitude was changed and on the length of time waited before the polarization was recorded.

The source of the error is best illustrated with a specific example. If $P_{\rm max}$ is 55% then the build-up time τ is 25.6 min, and 33 min are required for the polarization to build-up from 0 to 40%, and another 28 min from 40 to 50%. The rate of increase of the polarization can be found using eqs. (1) and (6):

$$\frac{{\rm d}P}{{\rm d}t}(t) = \left(\frac{P_{\rm ST}}{\tau_{\rm ST}}\right) {\rm e}^{-t/\tau}. \tag{25}$$

The rate decreases exponentially with time and in this example the rate is 0.20%/min when $P = 50\%$. If the amplitude of a correction is then changed, it may be difficult to interpret the effect from the measured polarization. For example, if the change increases $P_{\rm max}$ from 55 to 60%, then the rate of increase ${\rm d}P/{\rm d}t$ jumps from 0.20%/min to 0.36%/min. After waiting 20 min the polarization has risen to 55.2%, a difference of only 2.5% from the value obtained if one had just waited without changing the amplitude. This should be compared with the typical statistical error for a 5 min measurement of about $\pm 1.5\%$, achieved with an electron current of 1.5 mA.

This example illustrates how the systematic error in determining $P_{\rm max}$ at two successive amplitudes can distort the measurement of the dependence of $P_{\rm max}$ versus D: if the polarization is seen to increase after a correction is changed, it can be difficult to determine if the increase is the effect of the correction or a continuation of the build-up. Open symbols have been used in Fig. 10 to indicate values which are believed to be too low with respect to neighboring points (and can thus lead to a misinterpretation of the measured dependence of the polarization versus the amplitudes) because of build-up effects; this often occurred when the first point in a scan, typically at 0 mm, was measured after an injection.

The possible difficulties in the interpretation of the scans are illustrated with the measurements of the correction 0-Real, shown in Fig. 10a. The first portion of the scan was performed after a long period of stable conditions at 0 mm amplitude, while a problem with

the polarimeter was studied. The initial polarization was 48.6 ± 2.0%, and as the amplitude of the correction was increased the polarization was observed to decrease. The beam was lost shortly after the amplitude was returned to zero, and the scan was completed with a new fill of the electron ring. The time dependence of the polarization during the measurement of these six amplitudes is shown in Fig. 11. The amplitude of the correction at the time of injection was 0 mm, and was changed to −0.6 mm after about 1 h, and to −1.2 mm after an additional 20 min. At about 14:00 it was noticed that the voltage of a cavity had dropped, the exact time uncertain, and the cavity voltage was then restored to its initial value. The scan was continued to −2.4 mm, when it was clear that the optimum amplitude was closer to 0 mm. On the basis of these five points, one might conclude that the optimum amplitude is near −1.2 mm. But considering the measurements before the beam was lost, the loss of the cavity voltage which might have pushed the beam into a synchrotron resonance and the effects of the long build-up time, we have concluded that the optimum amplitude is near 0 mm. This conclusion is consistent with the results of a scan performed later, also shown in Fig. 10a.

In summary, measurements of the polarization as a function of a correction amplitude can be difficult to interpret when the build-up time is long. When near the maximum, where the effect of the correction is small, the effects of the long build-up can be misjudged as being due to the correction. It may also be difficult to extrapolate from measurements of the "sides" of the curve to the position of the maximum, if the dependence has been distorted or if the curve is very asymmetric. The systematic error ΔD_{opt} for the components of the 0 and +1 harmonics is estimated to be approximately 0.5 mm. As a result of the insensitivity of the polarization to the amplitudes of the −1 and +2 harmonics, the corresponding systematic error for these components is larger.

5.1.2. Closure of the bumps

The eight harmonic corrections are generated with a family of eight closed orbit bumps located in the arcs, Fig. 1. When gradient errors are located within a bump then the bump may not be closed, i.e. the bump will disturb the orbit of the beam around the entire machine. The nonlinear fields of the sextupoles in the bumps also disturb the closure, but estimates indicate that this effect should be small.

The change in the vertical position and angle of the electron beam at the position of the IP of the polarimeter can be monitored by measuring the mean vertical position of the backscattered photons at the detector, a quantity which is particularly sensitive to the vertical angle of the orbit. The mean position is monitored continuously to keep the distribution centered on the calorimeter; the typical displacement when the amplitude of a correction was changed, was small. In one case, a displacement of 300 μm was observed when the amplitude of the component 0-Imaginary was changed by 1 mm, which corresponds to a change of the vertical direction of the electron orbit at the IP of about 4.6 μrad mm of orbit correction amplitude.

A global measurement of the closure of the eight bumps was performed by measuring the orbit around the ring with position monitors, before and after the addition of a correction. A Fourier analysis of the difference between the orbits indicates an increase, due to the correction, in the harmonic component at the frequency of the vertical betatron oscillations. This shows that the bumps are not completely closed [29], but the effect is consistent with the expected influence of the sextupoles.

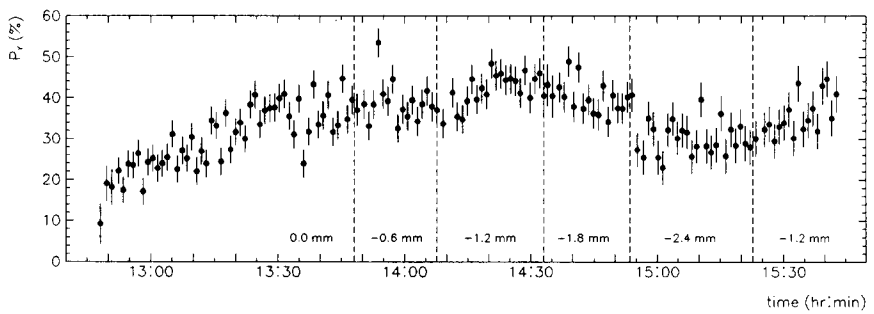

Fig. 11. The polarization plotted as a function of time (in approximately 1 min intervals) during the continuation (following injection) of the first scan of the harmonic correction 0-Real, shown in Fig. 10a. The time scale begins shortly after injection, and the approximate times when the amplitude was changed are indicated with dotted lines. The average of the last five measurements with each amplitude are plotted in Fig. 10a.

5.2. Other orbit corrections

The orbit corrections which are available to increase the polarization are not limited to the harmonic spin–orbit corrections, which are used to correct the rms tilt of $\hat{n}_0$. The effect on the polarization of the correction of the coupling of the vertical and horizontal betatron motions has also been studied. The coupling, believed to be an effect of the iron of the proton magnets on the stray fields of the electron magnets, produces a tilt (or rotation) of the cross sectional ellipse of the electron beam; a measurement at 12 GeV indicated a rotation of about 12°. Sextupoles are located within the bumps used for the spin–orbit correction (see Fig. 1), thus the tilt correction will also affect the coupling.

The coupling is compensated with a vertical "decoupling bump" in the arcs of the ring. During the measurements in November 1991 the decoupling bump was located in one octant and an amplitude of about 4.5 mm was required for the correction. The polarization was found to increase when this correction was used [2]. This has been understood on the basis of simulations with SITROS [30], which indicate that the reduction of the nonlinear depolarizing effects achieved by reducing the coupling compensates for the depolarizing effects of the bump due to the increase of the tilt of $\hat{n}_0$ and of the vertical dispersion.

As mentioned in section 1, the depolarizing effects of the decoupling bump were reduced by distributing it around the arcs. The amplitude thus required for the correction is about 0.5 mm. After the initial studies of the spin–orbit corrections, the dependence of the polarization on the tilt of the ellipse was measured. After changing the amplitude of the correction by about 0.2 mm, (corresponding to a rotation barely discernible on a synchrotron radiation monitor) the polarization was observed to increase from $33.7 \pm 1.4\%$ to $39.5 \pm 1.5\%$. The effect of the decoupling bump on the polarization will be studied again in future measurements.

As described in section 2.1.1, vertical dispersion can be a strong source of spin diffusion. Orbit corrections are available to minimize the vertical dispersion, but their effect on the polarization has not yet been measured.

To summarize this section we wish to reiterate that the orbit correction schemes were successful in increasing the polarization as predicted by calculations. The long build-up time together with typical statistical errors of 3% per minute at the available beam energy and current made a precise optimization time consuming. Thus the maximum polarization measured of $56.0 \pm 1.6\%$ ($\pm 5\%$ systematic) can be considered as a lower limit of the polarization value currently achievable. The electron current expected during the 1993 run period is significantly larger than the maximum current achieved in 1992. The build-up time at the design energy of 30 GeV (the operating energy of the spin rotators) is only half the value at 26.7 GeV. These improvements will reduce the difficulties with the optimization substantially.

6. Measurement of the build-up time

The measurement of the build-up time provides a check of the polarization scale with small systematic

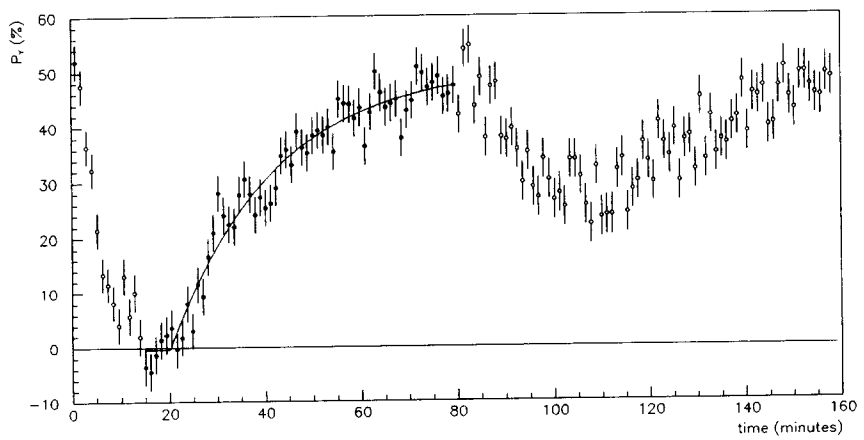

Fig. 12. The build-up of polarization after depolarization. Selected spin–orbit corrections were used to depolarize the beam. After the amplitudes were reset to zero, the polarization level rose for 1 h, until the loss of an accelerating cavity partially depolarized the beam. After the problem was fixed (at about $t = 110$ min) the polarization again began to rise. The results of the fit are: $P_{max} = 50.6 \pm 1.9\%$ and $\tau = 21.5 \pm 2.5$ min.

error. As can be seen by rearranging eq. (6),

$$P_{\max} = \tau\left(\frac{P_{ST}}{\tau_{ST}}\right), \tag{26}$$

and the asymptotic polarization $P_{\max}$ can be obtained from a measurement of τ.

One such measurement is shown in Fig. 12. The beam was depolarized by increasing the amplitudes of selected spin–orbit harmonic components until the polarization was lost. Then the amplitudes were put back to zero, and the polarization was allowed to build-up. After depolarization, the polarization rises in time according to (compare with eq. (1))

$$P(t) = P_{\max}\left[1 - \left(1 - \frac{P_0}{P_{\max}}\right) e^{-(t-t_0)/\tau}\right], \tag{27}$$

where t_0 is the time the build-up began and P_0 is the polarization achieved by the depolarization. During the measurement the beam was left depolarized only for a short time (less than 10 min). Due to the statistical fluctuation of the points for $t \approx 20$ min, the value of P_0 cannot be determined in a fit to eq. (27), and was determined by averaging the measured values for $15.2 < t < 20.6$ min. P_0 was thus found to be $-0.4 \pm 1.4\%$, and in the subsequent fit of the data to eq. (27) it was held fixed. The remaining free parameters of the fit are $P_{\max}$, τ, and t_0 and the results obtained are $50.6 \pm 1.9\%$, 21.5 ± 2.5 min and 20.3 ± 0.9 min, respectively, with the $\chi^2/\text{ndf} = 1.08$. On the basis of the values $\tau_{ST} = 43.2$ min and $P_{ST} = 91.6\%$ at HERA at 26.7 GeV [#3], the asymptotic polarization utilizing (26) is $P_{\max}(\tau) = 45.6 \pm 5.3\%$. This result is consistent (within the relatively large statistical error of 0.12 P_y), with the measurement of $P_{\max}$ determined in the fit to eq. (27), which utilizes eq. (22) and the estimates of $\Delta S_3 \Pi_\eta$ discussed in ref. [2]. Thus the "polarization scale", which is used to relate the measurements of $\Delta\eta$ to P_y, has been left unchanged and we continue to use the scale described in ref. [2]. The systematic error of the polarization measurement is estimated to be less than 0.10 P_y [2]. The higher electron currents which will be available during the next run period will enable a measurement of $P_{\max}(\tau)$ with a smaller statistical error and thus allow a better determination of the systematic error in the polarization scale.

7. Energy scans

The equilibrium polarization is a strong function of the beam energy, and a measurement of this dependence is important to determine the energy for maximum polarization, and for comparisons with predictions. In Fig. 13 we show the results of two partial energy scans. Unfortunately, it was not possible to perform a full scan under constant conditions. The step size was 5–10 MeV. The first scan was performed as part of the preparations for the orbit correction studies. The scan was interrupted twice by the loss of the electron beam. After a new injection, energy points were remeasured to check the reproducibility. The first scan extends to 26.720 GeV, with a maximum polarization of $25.5 \pm 1.5\%$ obtained at the energy of 26.700 GeV. The betatron tunes Q_x and Q_y were 47.14 and 47.20, respectively, and the synchrotron tune Q_s was 0.082. The second scan was performed near the end of the run period, after the completion of the correction studies. The maximum polarization measured was 43.6 $\pm$ 1.6%. This scan was also interrupted by the loss of the beam, and the betatron and synchrotron tunes were changed with the new fill: for the three points at the highest energy the tunes Q_x, Q_y and Q_s were 47.15, 47.21, and 0.071, respectively, and for the following portion of the scan the corresponding values were 47.12, 47.20, and 0.076.

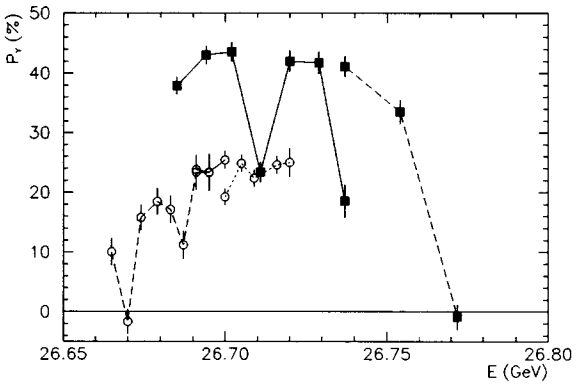

Fig. 13. Measurements of the polarization as a function of the beam energy. The first scan (○) was performed before the orbit correction studies. The scan was interrupted twice (dashed, solid, and dotted curves) and extends from 26.665 to 26.720 GeV. The second scan (□) was performed after the correction studies, and was interrupted once (solid, dashed curves). It extends from 26.685 to 26.772 GeV.

In Fig. 4 we show the results of simulations of a "typical" HERA ring before and after the optimization of the harmonic spin–orbit corrections have been performed. As discussed in section 2.4, the calculations are for a single simulation of the misalignments and of the conventional closed orbit corrections, and thus serve only as an indication of the expected polarization. The values taken for the tunes Q_x, Q_y and Q_s were 47.11, 47.19, and 0.072 respectively, which are slightly different than the measured values. The polarization peaks near the spin tune 60.5, and the width of

[#3] In HERA there are a small number of reversed-field dipoles.

the envelope is limited by the positions of the vertical betatron resonances ($m_y = \pm 1$; $\nu = 60.19$ and 60.82). The synchrotron sidebands add a fine resonance structure to the energy dependence. The spacing in spin tune, $\Delta\nu$, of the sideband resonances equals Q_s, which corresponds to a spacing in energy, ΔE, of 31 MeV. Sidebands of both first order vertical betatron resonances can be identified: for $m_y = 1$ and $1 \le m_s \le 4$ one expects resonances at $\nu = 60.26, 60.33, 60.41, 60.48$; for $m_y = -1$ and $-4 \le m_s \le -1$ one expects resonances at $\nu = 60.52, 60.60, 60.67$, and 60.74. The energies of the resonances depend only on the orbital tunes and the beam energy and thus can be accurately predicted; the dominant uncertainty is in the average beam energy, which is based on dipole field measurements and is known with an error of about ± 50 MeV. In contrast, the relative strengths of the resonances cannot be accurately predicted with simulations, due to the sensitivity of the strengths to the distribution of the magnet misalignments and to the closed orbit corrections.

Keeping in mind the difficulties of combining the incomplete and interrupted scans and comparing these with the results of the simulations, the data are overlaid on the Monte Carlo results in Fig. 14. A number of observations can be made:

– For the best fit of the two measured curves with the simulation results, the data have been shifted in energy by -64 MeV, consistent with the error in the energy scale. The shift estimated in the analysis of the November 1991 data was only -38 MeV (ref. [2], Fig. 30). The difference in the shifts of 26 MeV is approximately equal to the spacing of the sideband resonances, and is most likely a result of the uncertainty in determining the shift (by eye) for the optimum fit of the curves, and not from changes in the energy calibration of the machine.

– The measured maximum polarization before corrections of $25.5 \pm 1.5\%$ is in excellent agreement with the SITROS prediction of $26.0 \pm 6.0\%$ and also with the selected "typical" results. The maximum in the energy scan performed after the corrections is $43.6 \pm 1.6\%$, which is significantly lower than the SITROS prediction of $70.7 \pm 6.7\%$ and the maximum seen in the selected "typical" case. The values in this scan were recorded after waiting only about 25 min, and thus may be consistent with the maximum polarization measured during the run of $56.0 \pm 1.6\%$. The long build-up time with $P_{max} = 60\%$ and the non-optimum amplitudes of the corrections contribute to the difference between the measured and predicted maxima.

– The shape of the measured curve is consistent with the simulation results, with a flat-top of the polarization between 26.68 and 26.74 GeV (HERA energy scale, Fig. 13).

– The resonance structure of the synchrotron sidebands is visible in the measurements. As mentioned above, the strength of individual resonances cannot be predicted by the simulations. In addition, the betatron and synchrotron tunes used in the simulations are slightly different from the values measured during the data taking, thus the energy separation of the measured and predicted resonances cannot be expected to precisely agree. In spite of these caveats, a comparison of the resonance structures is informative. The spacing ΔE of the three "dips" in the first scan is about 20 MeV, and may indicate resonances. The dips in the second scan have an energy spacing, ΔE, of about 30 MeV, and may correspond to the $m_s = -3$, -4 and -5 sidebands of the first order Q_y resonance $m_y = -1$. Not unexpectedly, the strengths of the resonances in the simulations are not in good agreement with the measured values.

– The apparent resonances at 26.700 and 26.737 GeV (HERA energy scale, Fig. 13) were not reproduced when the points were repeated after a new injection. The reason may be the difference in the tunes for the two fills (particularly Q_s) which results in different energies of the resonances in the two scans.

In summary, the agreement between the measurements and the simulation results is encouraging. The interrupted scans could be combined due to the repro-

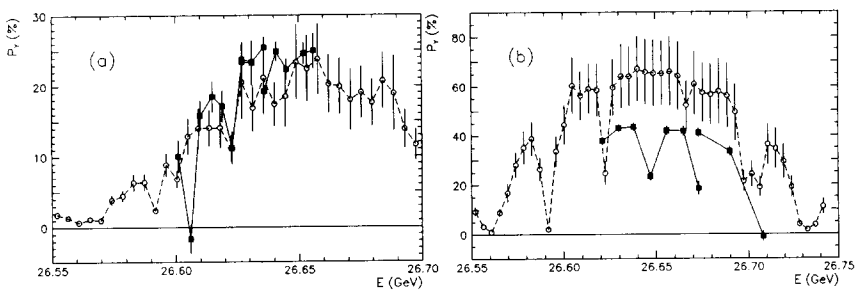

Fig. 14. Overlay of the simulation results (○) and measured values (□) of the polarization versus the beam energy, shown separately in figs. 4 and 13, respectively. In (a) are shown the values before optimization of the corrections, and in (b), after the optimizations. The data have been shifted in energy by -64 MeV.

ducibility of HERA from fill-to-fill. The measurement and interpretation of the data is complicated by the effects of the long build-up time; the systematic uncertainties may be reduced during the next run when higher electron currents are available, when it may be feasible to measure P_{max} as a function of energy by depolarizing at each point and measuring the build-up time. The SITROS program is proving to be a very useful tool, both for guidance and for interpretation of the measurements. A detailed comparison of the simulation results with the measured values has been hindered by the unknown error in the energy scale of the beam. The average energy of a polarized beam can be measured with great accuracy using the technique of resonant spin depolarization, utilized at LEP to measure the energy with a relative error $\Delta E/E$ of 10^{-5} [31]. With such an accurate measurement of the beam energy at HERA [32] individual synchrotron resonances could be identified and their strengths compared with predictions.

8. Conclusions

A vertical electron polarization of 8% was observed at HERA in November 1991. After the realignment of misaligned quadrupoles, a maximum polarization of about 18% was observed in the spring of 1992. During dedicated measurement time in August and September of 1992, special orbit correction schemes were tested and utilized to increase the polarization. The beam energy and the accelerating voltage were first tuned, and after the optimization of the harmonic spin–orbit corrections followed by a correction of the coupling, a maximum vertical polarization of $56.0 \pm 1.6 \pm 5\%$ (systematic) was achieved. The corrections will be fine-tuned in future measurements. The longitudinal component of the polarization was zero within the statistical error of about 1%. From the experience gained during the measurements, the polarization has been found to be very sensitive to many parameters (energy, accelerating voltage, etc.) but the short and long-term reproducibility of the ring is excellent. Polarization was observed during each measurement period in 1992: in April, June, August and September. After the initial optimizations in August, the optimum correction coil strengths were written into an optic file in the control system, and high levels of polarization were observed for later fills, without additional tuning, on the occasions that this file was used. Good reproducibility was observed from day-to-day, and also after the two weeks which separated the final measurement periods in 1992.

The build-up time was also measured, but due to the small bunch current, the statistical error on the result is large. It was possible to confirm, but not improve, the estimate of the systematic error in the polarization scale of less than 0.10 P_y. Comparisons have been possible (due to the excellent reproducibility of the machine) of measurements with the results of simulations of the polarization as a function of the beam energy. The agreement is encouraging, showing the predictive power of the SITROS program. A single scan covering a larger energy range with constant conditions is planned. The comparison of the results with predictions will be facilitated by an accurate measurement of the beam energy using resonant depolarization.

A high priority item during the next measurements will be to achieve polarization during luminosity operation, i.e. during the operation of the solenoids and compensators of the ZEUS and H1 detectors, the proton ring, and the multi-bunch feedback system. Spin rotators are being prepared for installation in the straight section East during the 1993/94 shutdown. Simulations indicate that with careful orbit corrections a high degree of polarization can also be achieved with spin rotators.

Acknowledgements

The authors would like to congratulate the HERA machine crew for the excellent performance of HERA and thank them for a productive collaboration. In particular, we would like to thank W. Bialowons for his interest and support. We are grateful for the support of the HERA Users for the polarization studies and for the use of beam time.

The help of F. Wedtstein with the programming of the software for the harmonic corrections is greatly appreciated; also the assistance of C. Kluth. Many people have contributed to the development and clarification of ideas for polarization optimization is storage rings, and we would like to take this opportunity to thank J.P. Koutchouk and R. Schmidt, and S. Mane for his early work on the FIDO program.

The interest of Prof. U. Camerini and the support of the University of Wisconsin are greatly appreciated and warmly acknowledged.

References

[1] J. Buon and K. Steffen, Nucl. Instr. and Meth. A 245 (1986) 248.

[2] D.P. Barber et al., Nucl. Instr. and Meth. A 329 (1993) 79.

[3] M. Düren, Polarization Measurements at HERA, presented at the 10th Int. Symp. on High Energy Spin Physics, Nagoya, Nov. 1992.

[4] A.A. Sokolov and I.M. Ternov, Sov. Phys. Doklady 8 (1964) 1203; and

I.M. Ternov, Yu.M. Loskutov and L.I. Korovina, Sov. Phys. JETP 14 (1962) 921.
[5] A.W. Chao, Nucl. Instr. and Meth. 180 (1981) 29; also in: Physics of High Energy Particle Accelerators, AIP Conf. Proc. 87 (1982) p. 395.
[6] Ya.S. Derbenev and A.M. Kondratenko, Sov. Phys. JETP 37 (1973) 968.
[7] S.R. Mane, Phys. Rev. A 36 (1987) 105.
[8] L.H. Thomas, Philos. Mag. 3 (1927) 1; and V. Bargmann et al., Phys. Rev. Lett. 2 (1959) 435.
[9] V.N. Baier, V.M. Katkov, and V.M. Strakhovenko, Sov. Phys. JETP 31 (1970) 908.
[10] B.W. Montague, Phys. Rep. 113 (1984) 1.
[11] K. Yokoya, KEK Report 92-6 (1992).
[12] J. Kewisch et al., Phys. Rev. Lett. 62 (1989) 419.
[13] M. Böge, in: DESY HERA 92-07, ed. F. Willeke (1992) p. 211.
[14] H. Mais and G. Ripken, DESY Report 83-062 (1983).
[15] D.P. Barber et al., DESY Report 85-044 (1985).
[16] E. Gianfelice-Wendt, DESY HERA 92-07, ed. F. Willeke (1992) p. 202.
[17] R. Rossmanith and R. Schmidt, Nucl. Instr. and Meth. A 236 (1985) 231.
[18] K. Nakajima, in: Proc. 3rd Europ. Part. Accel. Conf., Berlin, March 1992, eds. H. Henke, H. Homeyer and Ch. Petit-Jean-Genaz (Edition Frontières, 1993) p. 717.
[19] E. Gianfelice-Wendt, personal communication.
[20] S.R. Mane, DESY HERA 85-23 (1985).
[21] U. Fano, J. Op. Soc. Am. 39 (1949) 859.
[22] H. Götschel, diploma thesis, University of Hamburg, Germany, DESY F35D-90-01 (1990).
[23] R. Kaiser, diploma thesis, University of Münster, Germany, DESY F35D-92-02 (1992).
[24] W.R. Nelson, H. Hirayama and D.W.O. Rogers, SLAC-265 (1985).
[25] D. Westphal, diploma thesis, University of Hamburg, Germany, DESY F35D-93-04 (1993).
[26] M. Lomperski, DESY Report 93-045 (1993).
[27] A. Mücklich, diploma thesis, University of Heidelberg, Germany (1992).
[28] D. Proch et al., in: Proc. 15th Int. Conf. on High Energy Accelerators, Hamburg, July 1992, ed. J. Rossbach (World Scientific), Int. J. Mod. Phys. A (Proc. Suppl.) 2A (1993) p. 688.
[29] M. Sands, SLAC-0121 (1970); also in: Proc. Int. School of Physics, "Enrico Fermi", June 1969, ed. B. Touschek (Academic Press, 1971) p. 257.
[30] D.P. Barber, M. Böge and E. Gianfelice-Wendt, in: Proc. 15th Int. Conf. on High Energy Accelerators, Hamburg, July 1992, ed. J. Rossbach (World Scientific), Int. J. Mod. Phys. A (Proc. Suppl.) 2A (1993) p. 1088.
[31] L. Arnaudon et al., Phys. Lett. B 284 (1992) 431.
[32] M. Böge, presented at the 10th Int. Symp. on High Energy Spin Physics, Nagoya, Nov. 1992.